J. Membrane Biol. 187, 225–238 (2002)
DOI: 10.1007/s00232-001-0166-2

The Journal of
Membrane
Biology

Inhibition of Transiently Expressed Low- and High-Voltage-Activated Calcium Channels by Trivalent Metal Cations

A.M. Beedle, J. Hamid, G.W. Zamponi
Department of Physiology and Biophysics, University of Calgary, 3330 Hospital Dr NW, Calgary, Canada

Received: 24 October 2001/Revised: 6 February 2002

Abstract. Calcium channels are important regulators of neuronal excitability and contribute to transmitter release, calcium dependent gene expression, and oscillatory behavior in many cell types. Under physiological conditions, native low-voltage (T-type)- and high-voltage-activated (HVA) currents are potently inhibited by trivalent cations. However, the presence of multiple calcium channel isoforms has hampered our ability to unequivocally assess the effects of trivalent cations on channel activity. Here, we describe the actions of nine trivalent metal ions on transiently expressed α_{1G} (Cav3.1) T-type calcium channels cloned from human brain. In 2 mM external barium solution, yttrium most potently inhibited α_{1G} current (IC_{50} = 28 nM), followed by erbium > gadolinium ≈ cerium > holmium > ytterbium > neodymium > lanthanum ≫ scandium. With the exception of scandium, blocking affinity was loosely correlated with decreasing ionic radius. A detailed characterization of yttrium block revealed a 25-fold decrease in blocking affinity when the external concentration of charge carrier was increased from 2 mM to 20 mM. In 20 mM barium, yttrium also effectively inhibited various types of cloned HVA channels indicating that this ion is a nonselective blocker. For all calcium channels examined, yttrium preferentially inhibited inward over outward current, but block was otherwise voltage independent. In addition to peak current inhibition, P/Q- and L-type channels underwent a unique speeding of the macroscopic time course of inactivation. Whereas peak current block of α_{1A} channels was highly sensitive to the external charge carrier concentration, the inactivation effects mediated by yttrium were not, suggesting that the two effects are due to distinct mechanisms. Moreover, the speeding effect was greatly attenuated by manipulations that slowed the inactivation kinetics of the channels. Thus, our evidence suggests that yttrium effects are mediated by two distinct events: peak current block likely occurring by occlusion of the pore, and kinetic speeding arising from yttrium interactions with the channel that alter the state of the inactivation gate.

Key words: Voltage gated calcium channel — Low voltage activated — High voltage activated — Trivalent metal cation — Lanthanide — HEK cells

Introduction

Calcium influx through voltage-gated calcium channels mediates a number of unique functions in the central nervous system, including pacemaker activity, generation of low-threshold spikes, and neurotransmitter release (e.g., Deschenes, Roy & Steriade, 1982; Bal & McCormick, 1993; McCleskey, 1994; Magee & Johnston, 1995; Kim et al., 2001). Calcium channels are important pharmacological targets in the treatment of pain and certain forms of epilepsy (Tsakiridou et al., 1995; van Luijtelaar et al., 2000; Beedle & Zamponi, 2001; Kim et al., 2001) and have therefore been subjected to intense study. One area that has received considerable interest is their inhibition by divalent and trivalent metal ions, not only because nickel ions were once considered to be selective T-type calcium channel inhibitors, but also because these ions have a defined ionic radius and therefore constitute excellent structural probes of the permeation pathway. However, unequivocal interpretation of the data has been hampered by the presence of multiple calcium channel isoforms (e.g., Narahashi, Tsunoo & Yoshii, 1987; Akaike et al., 1989a; Magee & Johnston, 1995), and in the literature, a wide range of responses of native currents to divalent cations has been described. For example, reported IC_{50} values for

Correspondence to: G. Zamponi; email: zamponi@ucalgary.ca

nickel block of native calcium channels range from 47 to 600 μM (Narahashi et al., 1987; Akaike et al., 1989a; Akaike, Kostyuk & Osipchuk, 1989b; Todorovic & Lingle, 1998). Similarly, the reported potency of lanthanum (La^{3+})[1] inhibition ranges from IC_{50} values of 8 nM for block of high-voltage activated current in aortic smooth muscle cells (Akaike et al., 1989a) to 1.5 μM for block of low-voltage activated current in neuroblastoma cells (Narahashi et al., 1987). In addition, trivalent metal cation (M^{3+}) block has been reported to be both voltage dependent by some groups (Lansman, Hess & Tsein, 1986; Lansman, 1990; Block, Stacey & Jones, 1998) and voltage independent by others (Boland, Brown & Dingledine, 1991; Mlinar & Enyeart, 1993).

The cloning of calcium channel α_1 subunits such as the T-type calcium channel family, α_{1G} (Perez-Reyes et al., 1998; Cribbs et al., 2000; Monteil et al., 2000a), α_{1H} (Cribbs et al., 1998), and α_{1I} (Lee et al., 1999a; Monteil et al., 2000b); the N-type channel, α_{1B} (Dubel et al., 1992; Williams et al., 1992a); the P/Q-type channel, α_{1A} (Mori et al., 1991; Stea et al., 1994; Westenbroek et al., 1995); the R-type channel, α_{1E} (Zhang et al., 1993); and the L-type channels, α_{1C} (Mikami et al., 1989; Hui et al., 1991), α_{1D} (Snutch et al., 1991; Williams et al., 1992b), α_{1F} (Bech-Hansen et al., 1998), and α_{1S} (Ellis et al., 1988), has allowed detailed functional studies on these channel types in isolation. For divalent ions such as nickel, Lee and coauthors showed that α_{1H} channels are much more potently inhibited than those formed by α_{1G} (Lee et al., 1999b). However, little information about block of cloned calcium channels by trivalent cations has been reported to date.

Using transient transfection of tsA-201 cells, we can express identified calcium channels and conduct voltage-clamp studies under identical conditions. This is an ideal system in which to examine the actions of trivalent cations and to determine the usefulness of these ions as probes of the channel pore structure. Thus, we undertook a detailed study to clarify trivalent cation blocking effects on cloned calcium channels. We have cloned an α_{1G} channel construct from human brain tissues, transiently expressed it and other rat calcium channel cDNAs, and examined their inhibition by trivalent metal ions. Our data show that all trivalent metal ions tested, with the exception of scandium, are potent inhibitors of T-type channels with affinities in the submicromolar range, and that blocking affinity is loosely correlated with ionic radius. Whereas peak current inhibition was relatively nonselective among all types of calcium channels examined, P/Q-type and L-type channels underwent a speeding of inactivation kinetics that might be indicative of the presence of a second binding site outside of the pore region that is coupled to the inactivation machinery.

[1]Abbreviations: cerium, Ce^{3+}; erbium, Er^{3+}; gadolinium, Gd^{3+}; holmium; Ho^{3+}; lanthanum, La^{3+}; neodymium, Nd^{3+}; scandium, Sc^{3+}; trivalent metal cation, M^{3+}; ytterbium, Yb^{3+}; yttrium, Y^{3+}.

Materials and Methods

Calcium Channel Constructs

α_{1G}: Four different human α_{1G} constructs were cloned and combined to create a full-length α_{1G} channel. Fragment I was obtained by filter hybridization screening, according to manufacturer's protocol, of a human cerebellum library (Clontech) in λgt11. Similarly, fragment IV was retrieved from a human fetal brain library (gift from Dr. S. Kaneko, Kyoto University) by alternately screening with two radioactive probes. These probes for screening were created by PCR with the following primers: fragment I, sense 5′-TCATCGTCATCGCAGGGATGCTGGAG and antisense 5′-GTTCTCGCGTGGCTGGGAGCAG (designed from GenBank™ AF126965 sequence); fragment II, sense1 5′-TGCTTCTG AGCACCAGGACTGC, antisense1 5′-CATTTCAGCCAGAA AGACTGCG, sense2 5′-GAAGTGCTACAGCGTGGAGG, antisense2 5′-CCAGGTCTGCTGGGTCAGAGG (designed from GenBank™ AF029228 and AF029229 EST sequences). Probes were radiolabelled with α-^{32}P dCTP using T7 DNA polymerase (Pharmacia). Both clones were removed from lambda phage and inserted into pBluescript KS (Stratagene). Fragments II and III were obtained by RT-PCR of human neuroblastoma cell RNA (gift from Dr. M. Kelly, Dalhousie University) and inserted into pCR-Blunt vector from Invitrogen (primers: fragment II, sense 5′-TCATCGTCATCGCAGGGATGCTGGAG, antisense 5′-TCG CTGTGCTGGGCATCCTGTGTGAACTC; and fragment III, sense 5′-CCTCAACATCCCACCCGGGCCCTAC, antisense 5′-TCTGGGGCTGCTGGTAGTGCTCCAT). Both sense and antisense strands of all clones were sequenced by ABI PRISM standard automated sequencing with BigDye. Then fragments were joined sequentially using *Sal*I (clones I and II), *Bgl*II (clones II and III), and *BstE*II (clones III and IV) restriction sites and inserted into a modified PMT2 mammalian expression vector, via *Not*I and *Kpn*I (NEB), for transfection.

cDNA constructs encoding α_{1A}, α_{1B}, α_{1C} and α_{1E}, plus ancillary β and α_2-δ1 subunits were kindly provided by Dr. Terry Snutch.

CecCCC: In this ultra-slowly inactivating L-type channel mutant, a region encompassing the first two thirds of the domain I-II linker was replaced with corresponding α_{1E} sequence. The creation of this construct and its biophysical evaluation have been described previously by our laboratory (*see* Stotz & Zamponi, 2001).

Cell Culture and Transient Transfection

HEK tsA-201 cells were grown to 85% confluency at 37°C (5% CO_2) in Dulbecco's modified Eagle's medium (DMEM) containing 10% fetal bovine serum, 200 U/ml penicillin, and 0.2 mg/ml streptomycin (Life Technologies, Inc.). Cells were dissociated with trypsin (0.25%)-EDTA (1 mM) before plating at 8% confluency on glass coverslips. Calcium channel (6 μg) and green fluorescent protein marker (2 μg) DNA were transfected into cells with calcium phosphate. For T-type expression, only human α_{1G} and green fluorescent protein DNAs were necessary for expression; however, for all other calcium channels, the rat α_1 subunit + α_2–δ_1 + β_{1b} (or, if explicitly stated, β_{2a}) + green fluorescent channels protein were transfected. Cells were transferred to 28°C the day following transfection and stored for 1 or 2 days before recording.

Trivalent Cations

All trivalent cations (cerium(III) chloride heptahydrate, Ce^{3+}; erbium(III) chloride hexahydrate, Er^{3+}; gadolinium(III) chloride hexahydrate, Gd^{3+}; holmium(III) chloride hexahydrate, Ho^{3+}; lanthanum chloride heptahydrate, La^{3+}; neodymium(III) chloride hexahydrate, Nd^{3+}; scandium chloride hexahydrate, Sc^{3+}; ytterbium(III) chloride hexahydrate, Yb^{3+}; and yttrium chloride hexahydrate, Y^{3+}; Sigma-Aldrich, Canada) were purchased at 99.9% purity and stored in a dessicator. Stock solutions (10 mM) in H_2O were made fresh daily in polypropylene tubes to limit the formation of M^{3+} hydrolysis products or precipitates. Serial dilutions were then carried out in the appropriate external solution. Despite careful handling of all trivalent solutions, the exact concentration of M^{3+} may be less than expected given the possible formation of trivalent hydroxides species (Mlinar & Enyeart, 1993).

Electrophysiology and Data Analysis

Cells were transferred into an external bath solution of 2 mM barium (in mM: 2 $BaCl_2$, 1 $MgCl_2$, 10 HEPES, 40 tetraethylammonium chloride, 10 glucose, 105 CsCl, pH 7.2), 2 mM calcium (in mM: 2 $CaCl_2$, 1 $MgCl_2$, 10 HEPES, 40 tetraethylammonium chloride, 10 glucose, 105 CsCl, pH 7.2), or 20 mM barium (in mM: 20 $BaCl_2$, 1 $MgCl_2$, 10 HEPES, 40 tetraethylammonium chloride, 10 glucose, 65 CsCl, pH 7.2) at room temperature, immediately prior to recording. Borosilicate glass pipettes were pulled and polished to ~3 MΩ resistance (Sutter Instrument and Narishige) when filled with cesium methanesulfonate internal solution (in mM: 109 $CsCH_3SO_4$, 4 $MgCl_2$, 9 EGTA, 9 HEPES, pH 7.2). Data were acquired and filtered at 1 kHz by an Axopatch 200B amplifier and pClamp 8.0 software (Axon Instruments). Series resistance was compensated to 90% where necessary. Voltage-pulse protocols are described in the appropriate figure legends. Control or M^{3+}-containing bath solutions were perfused directly onto cells by a custom-built perfusion system, obtaining complete solution change in less than one second.

Data analysis and offline leak subtraction were carried out in Clampfit 8.0 (Axon Instruments) and all curves were fit using SigmaPlot 2000 (SPSS). Current–voltage (*I-V*) plots were fit by the expression $I = (V-E_{rev})G[(1/(1+\exp(-(V-V_a)/S)))]$ where E_{rev} is the reversal potential, G is the maximum slope conductance, V_a is the half-maximal activation potential, and S is the slope factor. Fit parameters cited in the text were obtained by fitting each individual $I-V$ curve and averaging the combined data. The chord-conductance (G) or activation were determined for each *I-V* plot (using E_{rev} described above) via $G = I/(V-E_{rev})$ and plotted as G/G_{max}. Individual inactivation and activation curves were fit with the Boltzmann equation, $P_{open} = X+(1-X)/(1+\exp(-z(V_h-V)/25.6))$; P_{open} is the fraction of maximal current, X is the non-inactivating fraction of current, z is the slope factor, and V_h and V are the half-inactivating (or half-activating) and conditioning potentials, respectively. All dose-response curves were plotted as semilogarithmic and the averaged data were fit by $(1-(I_B/I_C)) = 1/(1+([M^{3+}]/IC_{50})^{n_h})$ where I_B/I_C is the fraction of current blocked in the presence of trivalent, $[M^{3+}]$ is trivalent concentration, IC_{50} is the concentration which blocks current by 50%, and n_h is the Hill coefficient. Because ensemble data were fit instead of individual cell data, error values generated by SigmaPlot 2000 indicate fitting probabilities and not true standard error. Therefore, error values are not included for IC_{50} data. All averaged data are plotted as mean ± SEM. Statistical analysis was carried out using paired *t*-tests (SigmaPlot 2000), $p < 0.05$ is considered significant.

Results

Cloning and Characterization of Human A_{1G}

We cloned and assembled a full-length α_{1G} (Cav3.1) calcium channel construct from human brain tissues and cell lines. Comparison of the deduced amino-acid sequence of our α_{1G} isoform with other reports reveals that our clone is identical to the "b" splice variant (absence of 7-amino-acid exon 25B and 18-amino-acid exon 26 in the III-IV linker; GenBank™ accession number AF126965) reported by Monteil et al. (2000a). Although not used in the assembly of the full-length construct, we also detected the "bc" (Δexon25B; AF227747) and "bce" (+exon14, Δexon25B; AF227749) variants in human neuroblastoma and fetal brain library, respectively. Although not rigorously investigated, we did not find any fragments of the "a" variant (+exon25B; AF126966); this may indicate a splicing preference for $\alpha_{1G\text{-}b}$ in fetal and transformed cells.

Transient transfection of our cloned α_{1G} construct into tsA-201 cells resulted in robust inward currents in 2 mM barium (Fig. 1*A*). As seen in Fig. 1, the threshold of activation was near −60 mV, with peak occurring at −30 mV. This is also evident from inspection of the ensemble current voltage relation obtained from 16 cells (Fig. 1*B*). The mean half-activation potential obtained from the individual cells was −47.5 ± 1.0 mV with a mean slope factor of 4.1 ± 0.3. The activation kinetics of the current were found to be steeply voltage dependent as evident from a decrease in the time to peak with increasing membrane depolarization. The time constant of inactivation, τ_h, measured by fitting the decay of the current waveform with a single exponential, was voltage dependent in the range between −60 to −30 mV, with no further change in kinetics at more depolarized potentials (Fig. 1*C*). This may reflect the strong voltage dependence of activation rather than any innate voltage dependence of inactivation kinetics (Serrano, Perez-Reyes & Jones, 1999).

Examination of steady-state inactivation shows that inactivation is first detectable at −90 mV and only 50% of current is available by −79.2 mV. When inactivation and activation curves are plotted together (Fig. 1*D*), a small region of overlap, near −60 mV, is observed. This window current is physiologically significant, as it indicates that a small fraction of channels are available to open with only small depolarizations above resting membrane potential. Current recovery from inactivation was both voltage- (Fig. 1*E*) and time-dependent (Fig. 1*F*) with half of the current recovering upon a 5-sec repolarization to −69 mV, and full current recovery by 1sec at −120 mV. Overall, the biophysical characterization of our α_{1G} clone exhibits the hallmarks of typical T-type

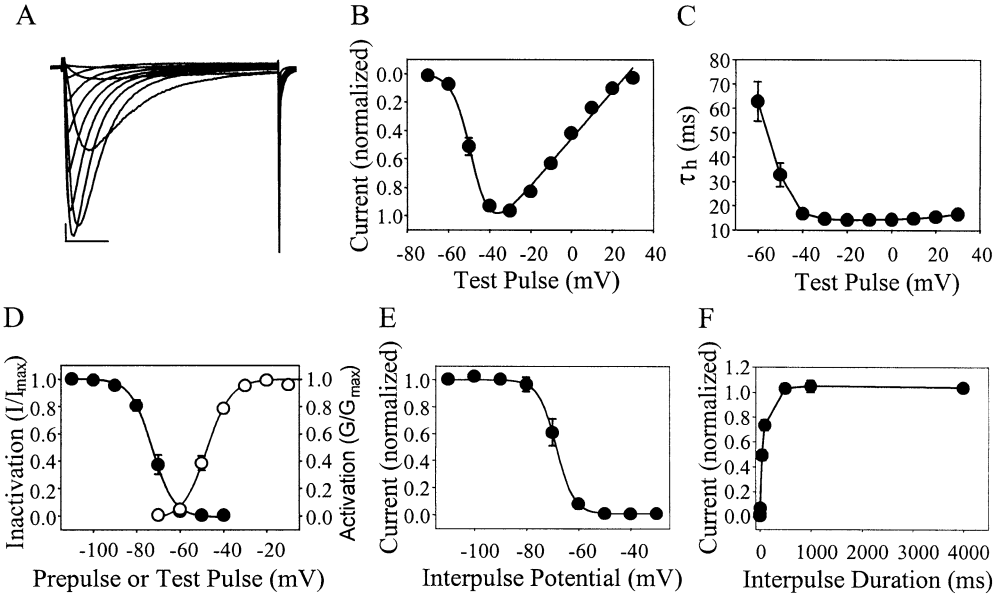

Fig. 1. α_{1G} expression in human embryonic kidney (tsA 201) cells. (*A*) A typical family of α_{1G} T-type currents evoked in 2 mM barium external solution. Depolarizing voltage pulses starting from −70 mV and increasing in 10-mV increments were used to activate T-type current from a holding potential of −100 mV. Note the typical "cross-over" waveform. Scale bars indicate: 100 pA, vertical; and 30 msec, horizontal. (*B*) Normalized peak α_{1G} current is plotted against test-pulse voltage and fitted as described in Materials and Methods. The half-activation potential obtained from the ensemble fit (*solid line*) was −50 mV. (*C*) The decay rate or τ_h was determined by fitting each waveform (as in *A*) from current peak to the end of the pulse with a single-exponential decay ($n = 10$). Note that the rate of current decay shows strong voltage dependence at potentials more negative than −40 mV. (*D*) Voltage dependence of inactivation and activation are plotted. Steady-state inactivation (*filled circles*) was assessed via 5-sec inactivating prepulses beginning at −120 mV (increasing in +10-mV increments), before a −30 mV test pulse to assess available current. Data are plotted as test pulse I/I_{max} versus prepulse potential ($V_h = -79.2 \pm 1.0$ mV; $z = 7.0 \pm 0.4$; $n = 14$). For α_{1G} activation (*G*; open circles), data from *B* was transformed and plotted as G/G_{max}. (*E*) The voltage dependence of α_{1G} recovery from inactivation was assessed using the following protocol: 5-sec pulse to −20 mV to inactivate α_{1G}, 5-sec interpulse ranging from −120 to −30 mV, test pulse to −30 mV to assess current recovered. Test pulse I/I_{max} versus interpulse potential shows that in 5 sec, half of α_{1G} current recovers at -69 mV ($n = 8$). (*F*) The time-dependence of α_{1G} recovery from inactivation was tested by applying a 5-sec pulse to +20 mV to inactivate α_{1G}, followed by an interpulse of −120 mV varying from 2 to 6000 msec. Available current was measured by a test pulse to −30 mV. Under these conditions, all α_{1G} inactivation recovers within 500 to 1000 msec ($n = 8$).

calcium channels and closely parallels the properties of human and rat α_{1G} calcium channels identified previously (Perez-Reyes et al., 1998; Monteil et al., 2000a; McRory et al., 2001).

Current–voltage relations and inactivation curves were also measured in 20 mM external barium. As expected, the increase in charge carrier concentration induced a positive shift in both activation and inactivation parameters ($V_a = -43.3 \pm 1.4$, $n = 15$; $V_h = -65.6 \pm 0.9$, $n = 11$). However, given the increased driving force in 20 mM barium, obtaining well-clamped currents can become a challenge.

Therefore, all trivalent experiments were conducted in 2-mM barium unless explicitly stated otherwise.

Trivalent Cations Block A_{1G}

To determine the inhibitory profiles of M^{3+} on an identified T-type calcium channel species in isolation, we applied various concentrations of a series of nine trivalent metal ion species to α_{1G} channels expressed transiently in tsA-201 cells. Fig. 2*A* displays representative waveforms obtained in the absence and presence of 100 nM for two of the lanthanides (Nd^{3+} and Er^{3+}) and three of the non-lanthanides (Sc^{3+}, Y^{3+} and La^{3+}) in the bottom traces and top traces, respectively. As seen from the figure, the application of 100 nM of each of the blocking ions produced varying effects on T-type channel activity, with Y^{3+} mediating almost complete block, whereas the same concentration of Sc^{3+} resulted in little if any inhibition. Block was dose-dependent and often reversible, albeit slowly, following washout (Fig. 2*B*). Fig. 2*C* illustrates dose response curves for all of the blocking ions considered in this study. As seen from Fig. 2*C*, the lanthanides all blocked in a similar range of concentrations with their IC_{50}s falling between the non-lanthanide La^{3+} and Y^{3+} ions. Of all the ions examined, Y^{3+} mediated the most pronounced inhibition with an affinity in the low nanomolar range ($IC_{50} = 28$ nM). On the other hand, Sc^{3+} was by far the weakest M^{3+} species ($IC_{50} = 3.8$ μM). This could be attributed to the fact that the Sc^{3+} radius is much

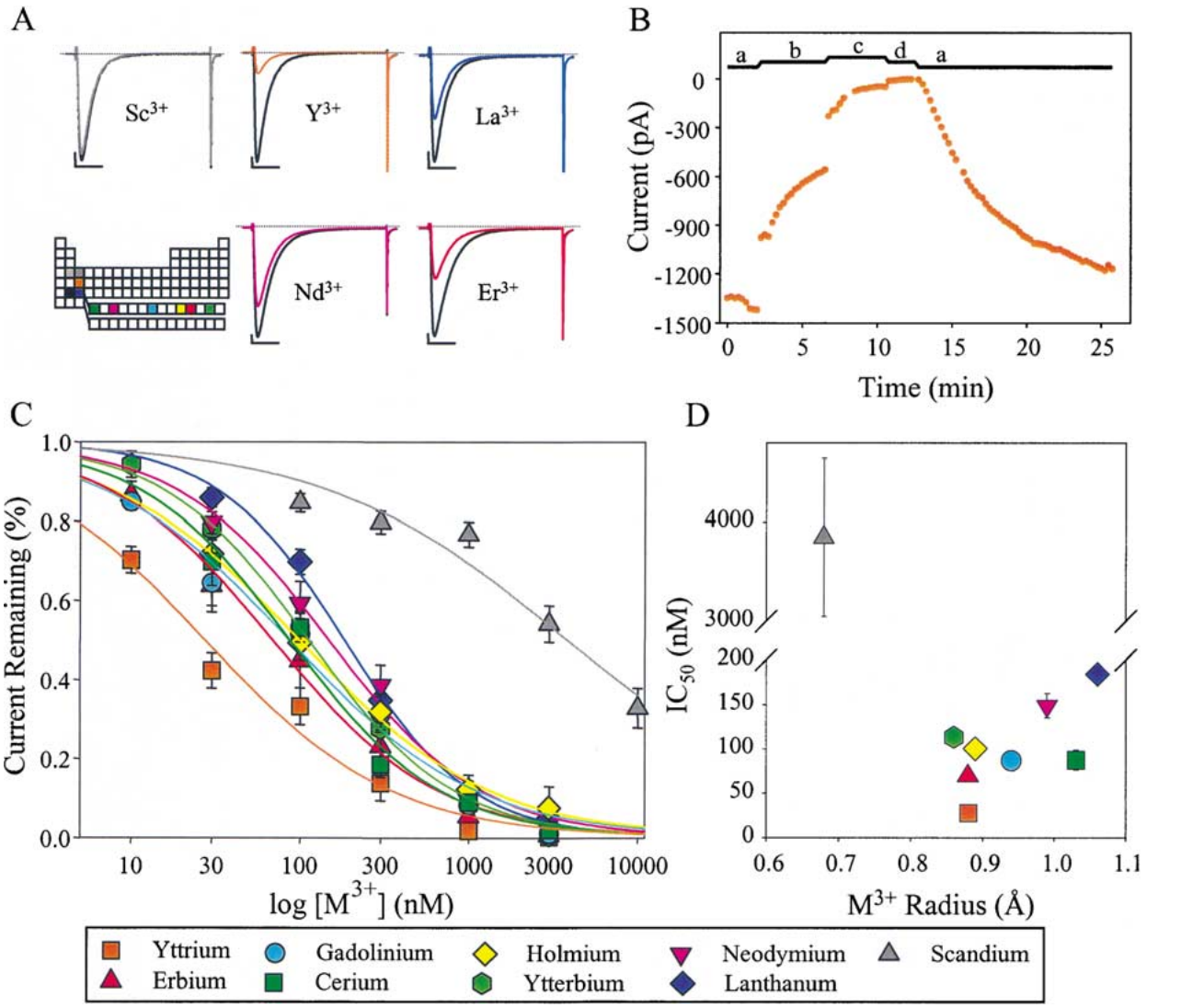

Fig. 2. Trivalent cation block of α_{1G} T-type currents (in 2 mM barium external solution). (*A*) Currents were evoked by steps to −30 mV from −100 mV under control conditions and in the presence of 100 nM M^{3+} (color coded according to M^{3+} species). To facilitate comparison, all M^{3+} species tested are shown on a small periodic table (*bottom left*). Trivalents from both row IIIB and the lanthanide series were tested; the positions of calcium (*light gray*) and barium (black) are also indicated. Horizontal scale bars mark 30 msec and vertical scale bars show 100 pA for all current traces. Current baselines are marked with dotted lines. (*B*) Representative time course of Y^{3+} block. Peak current was measured at 15-sec intervals. Small letters indicate different solutions: *a*, control/wash (2 mM barium); *b*, 30 nM Y^{3+}; *c*, 300 nM Y^{3+}; *d*, 3 μM Y^{3+}. Note that the blocking effect almost completely recovers following washout. The small amount of unrecovered block remaining at the end of the experiment is likely due to the fact that washout had not yet reached plateau (i.e., exponential extrapolation of the data predicts complete recovery). (*C*) Dose-response data are plotted on logarithmic scale for all trivalent metals tested. Data were fitted with the Hill equation to determine IC_{50}. Y^{3+} was the most potent inhibitor of α_{1G} (IC_{50} = 27.6 nM, Hill coefficient (n_h) = 0.8) followed by Er^{3+} (IC_{50} = 69.2 nM, n_h = 0.9), Gd^{3+} (IC_{50} = 86.6 nM, n_h = 0.8), Ce^{3+} (IC_{50} = 87.4 nM, n_h = 1.0), Ho^{3+} (IC_{50} = 99.8 nM, n_h = 0.8), Yb^{3+} (IC_{50} = 112.8 nM, n_h = 1.0), Nd^{3+} (IC_{50} = 148.4 nM, n_h = 1.0), La^{3+} (IC_{50} = 184.0 nM, n_h = 1.1), and Sc^{3+} (IC_{50} = 3846.3 nM, n_h = 0.6). Numbers of determinations per data point ranged from 5 to 12. In order to facilitate comparison among the M^{3+} species, additional data points at lower Y^{3+} concentrations are not shown in this figure but were included in fitting the Y^{3+} data. (*D*) Trivalent metal blocking affinity is weakly dependent on M^{3+} radius (radii values obtained from Cotton et al., 1995).

smaller and that Sc^{3+} chemical properties are much less "calcium-like" than the other M^{3+} tested (Cotton et al., 1995). Considering the small size of Sc^{3+}, and the finding that certain small monovalent cations (particularly Li^+ and Na^+) are permeable through calcium channels in the absence of divalent cations (Hess, Lansman & Tsien, 1986), we tested whether Sc^{3+} could also permeate the calcium channel. We perfused cells with a 2 mM Sc^{3+} solution (no barium or calcium); however, no inward current could be detected (n = 4, *data not shown*), suggesting that Sc^{3+} permeates the channel poorly or not at all.

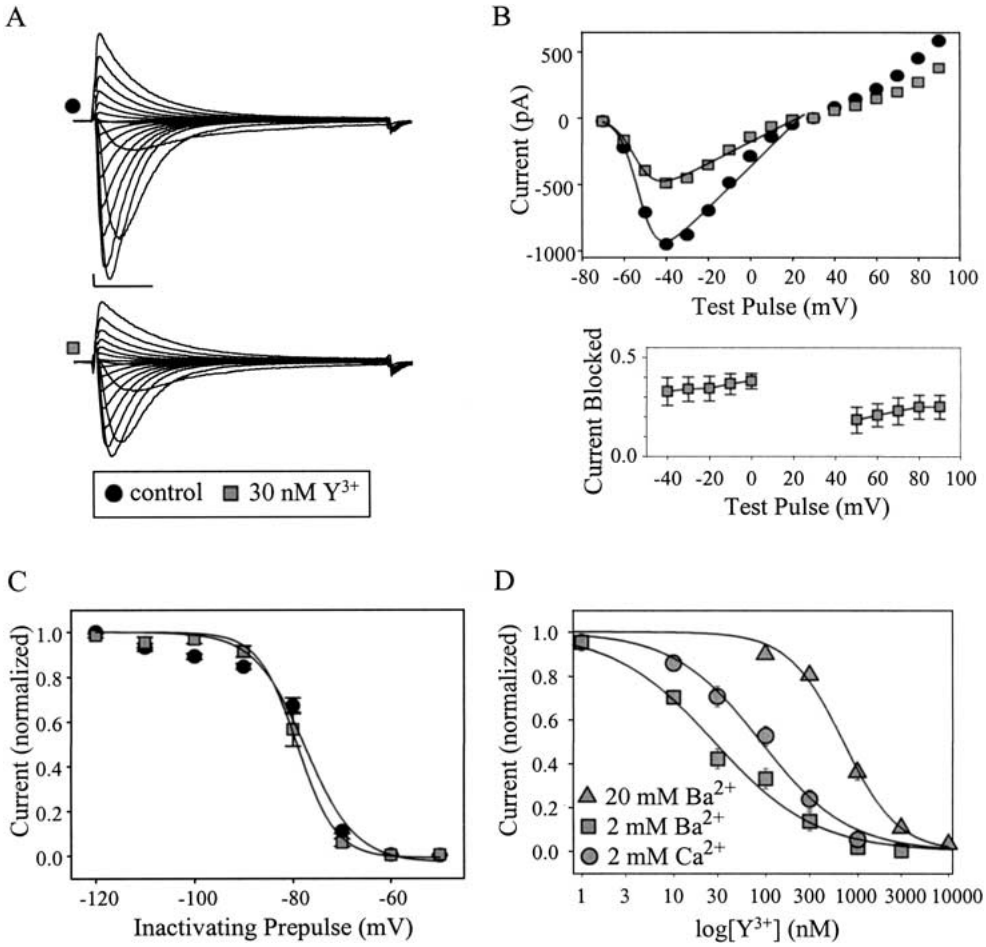

Fig. 3. Characterization of Y^{3+} block of α_{1G} currents. (*A*) A typical family of currents is shown under control conditions (2 mM barium external) and in the presence of 30 nM Y^{3+} (scale bars: horizontal, 30 msec; vertical, 100 pA). Currents were evoked as described in Fig. 1*A*. (*B*) Top panel: representative current–voltage relations are plotted in the absence and presence of 30 nM Y^{3+} (control: $V_a = -54$ mV; 30 nM Y^{3+}: $V_a = -56$ mV). In the lower panel, fractional current block is shown for the data set ($n = 5$). Note that inward current (−40 to 0 mV) is blocked more potently than outward current (+50 to +90 mV). (*C*) Inactivation curves are plotted in the absence and presence of 30 nM Y^{3+} (control: $V_h = -77.5$ mV; 30 nM Y^{3+}: $V_h = -79.1$ mV; $n = 5$). (*D*) Y^{3+} block is sensitive to the type and concentration of external charge carrier. Y^{3+} in 2 mM barium external solution is most effective. The data were fitted with the Hill equation, (data from Fig. 2*C*, $IC_{50} = 27.6$ nM, $n_h = 0.8$; Y^{3+} in 2 mM calcium: $IC_{50} = 88.9$ nM, $n_h = 0.9$; Y^{3+} in 20 mM barium: $IC_{50} = 700.1$ nM, $n_h = 1.4$; $n = 7, 10$).

When the potency of M^{3+} cations (excluding Sc^{3+}) was compared to size, a loose inverse correlation with ionic radius could be observed (Fig. 2*D*), suggesting that the size of the ions may be a contributing factor to blocking affinity.

To further characterize M^{3+} block of α_{1G}, we examined the voltage dependence of activation and inactivation in the presence and absence of the most potent blocker, Y^{3+}. At half-maximal concentrations of Y^{3+} (i.e., 30 nM; Fig. 3*A*, *B*), we detected neither a significant shift of the voltage dependence of activation (control: $V_a = -54.4 \pm 1.6$ mV; 30 nM Y^{3+}: $V_a = -55.7 \pm 1.7$ mV; $n = 5$, $p = 0.23$), consistent with a lack of significant screening of surface charges induced by the presence of 30 nM external trivalent cations, nor significant voltage-dependence of blocking action (*see below*). Inward barium current was blocked more potently than outward cesium current (Fig. 3*B*, lower panel), indicating that the direction of current flow and/or the species of permeating ion are determinants of blocking affinity, which is consistent with a site of action in the pore region of the channel. Over a range of test potentials (omitting currents near E_{rev}), Y^{3+} block of inward current did not, however, appear to exhibit any detectable voltage dependence, suggesting that, if block were to occur within the permeation pathway, Y^{3+} ions do not enter deeply into the transmembrane electric field. The position of the steady-state inactivation curve was not significantly affected by 30 nM Y^{3+} when compared to time-dependent controls (Fig. 3*C*; control: $\Delta V_h = -0.7 \pm 0.4$ mV; 30 nM Y^{3+}: $\Delta V_h = -1.7 \pm 1.0$ mV, $p = 0.32$).

If Y^{3+} block were to occur via physical occlusion of the pore, one would expect that raising the con-

centration of external permeant carrier ion would competitively antagonize Y^{3+} inhibition. We thus compared Y^{3+} inhibition in 2 mM and 20 mM barium external solutions. Block by Y^{3+} underwent a dramatic 25-fold reduction with this 10-fold increase in barium (Fig. 3*D*). Although this decrease in affinity is, in principle, consistent with a competition between the permeating barium ions and Y^{3+}, a 25-fold difference is too large to be exclusively due to such a mechanism, and it is likely that the increased surface-charge screening in 20 mM external barium may reduce the effective concentration of Y^{3+} near the blocking site. Therefore, to circumvent the issue of surface-charge screening, we recorded the effects of Y^{3+} in 2 mM external calcium, which does not involve a change in the external divalent cation concentration, and thus eliminates diffuse screening effects. As seen in Fig. 3*D*, the Y^{3+} inhibition of α_{1G} current was decreased more than 3-fold when barium was replaced by calcium as the charge carrier (Fig. 3*D*). Since calcium ions are thought to show a higher affinity for the channel pore compared with barium ions (Lansman et al., 1986), these data are consistent with competition between Y^{3+} and the carrier ion in the pore. Overall, our data suggest that trivalent metal ions do indeed block in the pore, but that their blocking affinity is strongly influenced by negative surface charges on the extracellular face of the channel.

Y^{3+} Inhibits High-Voltage-activated Calcium Channels

To determine whether Y^{3+} block is specific for T-type calcium channels, we tested the effects of Y^{3+} on transiently expressed rat N-type (α_{1B}), L-type(α_{1C}), P/Q-type (α_{1A}) and R-type (α_{1E}) calcium channels (co-expressed with ancillary α_2-δ_1 and β_{1b} submits). Because L-type calcium channels do not, in our hands, yield sufficiently large currents in 2 mM external carrier solution, we carried out all of the recordings in 20 mM external barium. Figs. 4*A* and *B* compare the effects of 1 μM Y^{3+} on the activities of different calcium-channel isoforms. Representative current-voltage plots (Fig. 4*A*, *upper panel*) and current waveforms in the presence and absence of 1 μM Y^{3+} (Fig. 4*B*, *upper panel*) are shown for each channel type. In combined data, R-type α_{1E} channels showed a slight, but significant negative shift in half-activation potential, whereas the half-activation potentials of other channel types remained unchanged (α_{1A} control: $V_a = -8.8 \pm 2.8$ mV; 1 μM Y^{3+}: $V_a = -6.7 \pm 1.4$ mV, $p = 0.41$. α_{1B} control: $V_a = 5.8 \pm 1.5$ mV; 1 μM Y^{3+}: $V_a = 3.8 \pm 1.7$ mV, $p = 0.22$. α_{1C} control: $V_a = -5.3 \pm 1.3$ mV;1 μM Y^{3+}: $V_a = -5.4 \pm 1.6$ mV, $p = 0.9$. α_{1E} control: $V_a = -14.9 \pm 1.2$ mV; 1 μM Y^{3+}: $V_a = -18.1 \pm 1.5$ mV, $p = 0.03$; $n = 5$). As with T-type current, HVA barium currents were more sensitive than outward cesium current to block by Y^{3+} (Fig. 4*A*, lower panel), but block otherwise appeared to be voltage independent.

Complete dose-response data in 20 mM external barium for all channel types tested reveal half-maximal blocking affinities by Y^{3+} ranging from 276 nM with α_{1E} to 769 nM with α_{1A} (Fig. 4*C*), suggesting that Y^{3+} is not a selective T-type calcium channel inhibitor and that different types of HVA calcium channels are similarly affected. However, upon closer inspection of the data, one interesting difference was noted. Whereas the presence of Y^{3+} did not affect the macroscopic time course of inactivation seen with T-type, N-type and R-type calcium channels over a range of Y^{3+} concentrations, inactivation of the P/Q-type and to a lesser extent, L-type channels, underwent a significant speeding in the presence of Y^{3+} (Fig. 4*B bottom row*, Fig. 4*D*). This effect was not voltage-dependent, as the ratio of the time constants for inactivation obtained in the absence and the presence of 1 μM Y^{3+} did not vary with test potential for any of the channels examined ($n = 5$ per channel, *not shown*). We also tested whether Y^{3+} influenced steady-state inactivation of α_{1A} and α_{1C} channels, but found no significant difference between the shifts in half inactivation potentials in 1 μM Y^{3+} and timed controls (α_{1A} control: $\Delta V_h = -6.3 \pm 1.7$; 1 μM Y^{3+}: $\Delta V_h = -9.1 \pm 3.0$, $p = 0.49$. α_{1C} control: $\Delta V_h = -3.3 \pm 1.4$; 1 μM Y^{3+}: $\Delta V_h = -4.6 \pm 1.6$, $p = 0.58$; $n = 6$ to 10). These data indicate that the observed Y^{3+} speeding effect is not influenced by membrane voltage, suggesting that it may be mediated at a site of action that is outside of the transmembrane electric field.

Y^{3+} Speeds the Inactivation Kinetics of A_{1A} and A_{1C}

The effect of Y^{3+} on the rate of current decay seen with L-type and P/Q-type channels could in principle be due to one of two different effects: 1) open-channel block developing during the test depolarization, similar to what we described recently for farnesol-related compounds (Roullet et al., 1999; Beedle & Zamponi, 2000), or 2), a true effect on inactivation gating. To discriminate between these alternatives, we examined the dose dependence, external charge-carrier dependence, and β-subunit dependence of Y^{3+} effects on P/Q-type currents. P/Q-type channels formed by either $\alpha_{1A} + \beta_{1b} + \alpha_2$-$\delta_1$ or by $\alpha_{1A} + \beta_{2a} + \alpha_2$-δ1 underwent dose-dependent peak current inhibition with Y^{3+} (Fig. 5*A*, *B*). Similar to our finding with T-type channels, the IC_{50} for Y^{3+} on block of peak current amplitude of α_{1A} channels increased more than 15-fold (from 45 nM to 769 nM) when external charge-carrier concentration was increased

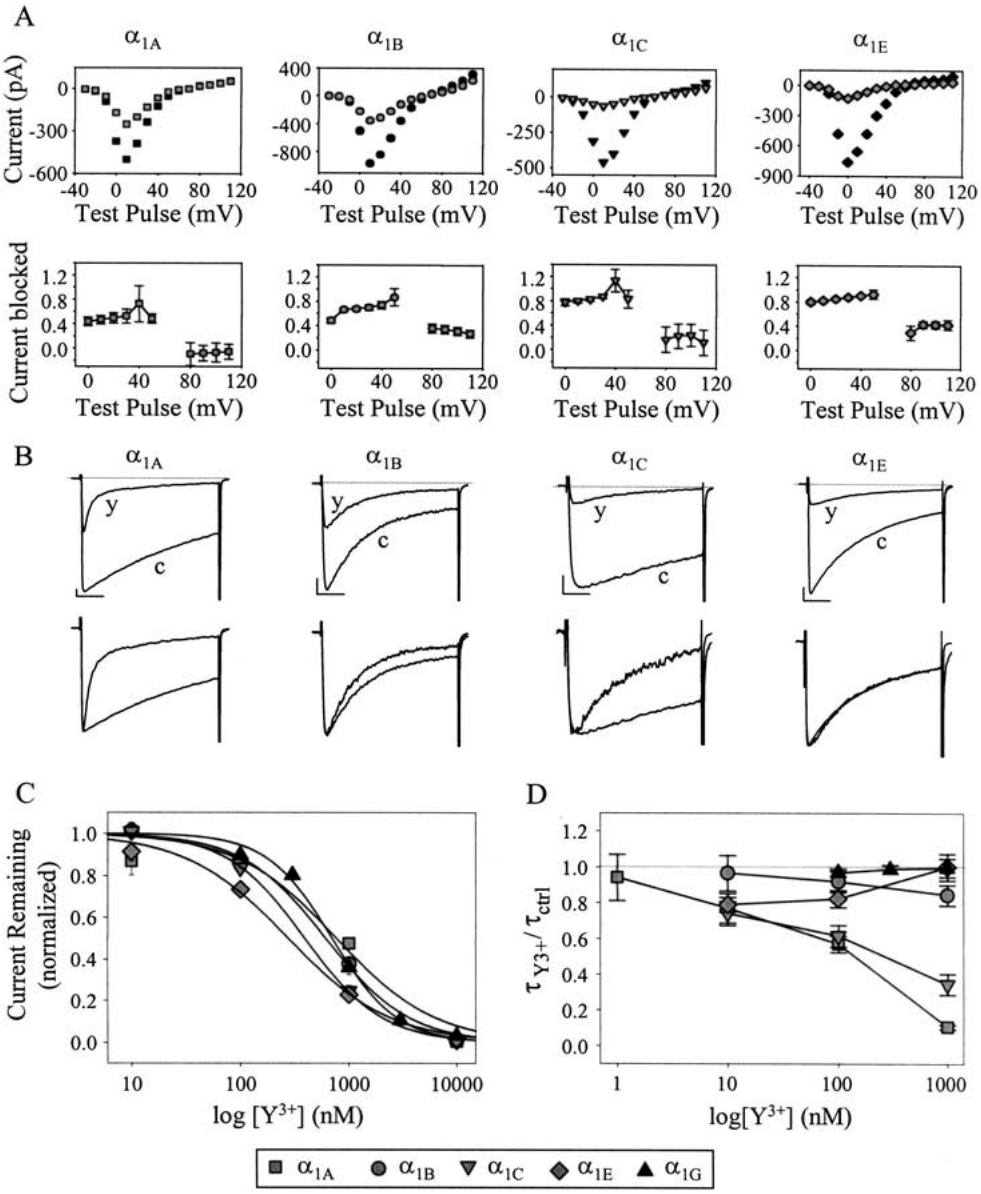

Fig. 4. Y^{3+} block of high-voltage-activated calcium channels in 20 mM barium. (*A*) The voltage dependence of Y^{3+} peak current block was measured by steps starting from −30 or −40 mV and increasing in +10-mV increments (V_{hold} = −100 mV). In the upper panel, representative current-voltage plots are shown for each high-voltage-activated channel subtype (control: black filled symbols; 1 μM Y^{3+}: gray filled symbols). Mean peak current block by 1 μM Y^{3+} at various test potentials is plotted in the lower panel (n = 5). Like α_{1G}, inward current is more potently inhibited than outward current for the high-voltage-activated channels. (*B*) *Top row:* Representative traces show control current, "c", and current remaining in the presence of 1 μM Y^{3+}, "y", for the P/Q-type (α_{1A}), N-type (α_{1B}), L-type (α_{1C}), and R-type (α_{1E}) calcium channels. All currents were evoked by a step depolarization to +10 mV. The scale bars reflect 30 msec (horizontal) and 100 pA (vertical). *Bottom row:* The traces have been scaled to the same peak to illustrate Y^{3+}-induced changes in the rate of current decay. (*C*) Dose-response data for peak current block by Y^{3+}. The dose-response curve for Y^{3+} block of T-type channels in 20 mM external barium (from Fig. 3*D*) is included for comparison. Y^{3+} effects on peak current are relatively nonselective among calcium channel subtypes (α_{1A}: IC_{50} = 768.7 nM, n_h = 1.0, n = 4 to 11. α_{1B}: IC_{50} = 611.9 nM, n_h = 1.1, n = 5 to 13. α_{1C} IC_{50} = 391.2 nM, n_h = 1.2, n = 6 to 12. α_{1E}: IC_{50} = 275.5 nM, n_h = 0.9, n = 6 to 12. α_{1G}: 700.1 nM, n_h = 1.4, n = 5 to 10). (*D*) The rate of current decay, τ, was obtained from monoexponential fits to the raw data and the ratio of τ_{Y3+} to $\tau_{control}$ is plotted (n = 6 to 12). There is a dose-dependent speeding of current decay when Y^{3+} is applied to P/Q-type (α_{1A}) and L-type (α_{1C}) calcium channels, but not to any of the other channel types examined.

from 2 to 20 mM, consistent with a combination of pore block and charge-screening effects (Fig. 5*B*). Interestingly, the effects of Y^{3+} on the rate of current decay became evident at concentrations at which no significant inhibition of peak current amplitude could yet be observed, and appeared to be independent of external barium concentration (Fig. 5*C*). Moreover, the speeding effect developed more rapidly following

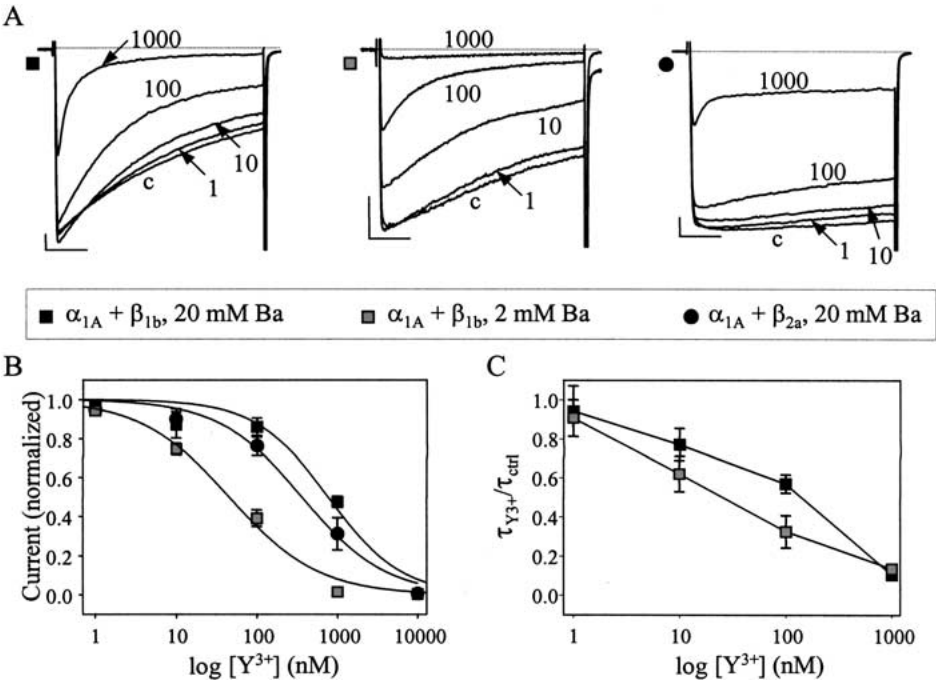

Fig. 5. Effects of Y^{3+} on P/Q-type calcium channels. (*A*) Representative traces obtained with α_{1A} channels evoked by stepping from −100 to +10 mV in the absence (*c*) and presence of various concentrations of Y^{3+} (numbers indicate [Y^{3+}] in nM). Note that Y^{3+} can affect current decay at concentrations lower than those required for a reduction in peak current amplitude for $\alpha_{1A} + \alpha_2$-$\delta_1 + \beta_{1b}$ channels in both 2 and 20 mM Ba (*left and center traces*). The presence of the rat β_{2a} subunit modulates Y^{3+} action (*right trace*). The scale bars reflect 30-msec (horizontal) and 100 pA (vertical). (*B*) Dose-response curves for peak current amplitude inhibition of α_{1A} channels coexpressed with either β_{1b} or β_{2a}. The data were fitted with the Hill equation, the parameters obtained from the fits were as follows: $\alpha_{1A} + \alpha_2$-$\delta_1 + \beta_{1b}$, 20 mM Ba: IC_{50} = 768.7 nM, n_h = 1.0. $\alpha_{1A} + \alpha_2$-$\delta_1 + \beta_{1b}$, 2 mM, Ba: IC_{50} = 45.4 nM, n_h = 0.8. $\alpha_{1A} + \alpha_2$-$\delta_1 + \beta_{2a}$, 20 mM Ba: IC_{50} = 360.1 nM, n_h = 0.8 (n = 5 to 11). (*C*) Effect of Y^{3+} on the macroscopic time constant of inactivation. $\tau Y^{3+}/\tau_{control}$ was obtained from monoexponential fits to the raw data in either 2 mM or 20 mM external barium. Note that the speeding of inactivation increases with increasing Y^{3+} concentration, and that this effect is largely independent of external charge-carrier concentration.

Y^{3+} application than the reduction in peak current amplitude (*not shown*). Overall, this suggests that this speeding effect must occur via a site that is distinct from that responsible for the Y^{3+}-induced peak current reduction.

Assuming that the tonic inhibition (i.e., the reduction in peak current amplitude) is due to simple pore block, this raises the possibility that the effect on the rate of current decay is not due to pore block, but instead due to an interaction with the inactivation machinery of the channel. Thus, manipulations that antagonize inactivation would be expected to selectively inhibit the effects of Y^{3+} on current kinetics. Calcium channel inactivation is strongly influenced by the species of β subunit coexpressed. To determine whether slower basal inactivation kinetics could influence the observed Y^{3+}-induced speeding of the current-decay rate, we compared the effects of Y^{3+} on channels coexpressed with either the rat β_{1b} subunit, or the rat β_{2a} subunit, which is known to antagonize voltage-dependent inactivation of all types of high-voltage-activated calcium channels (Restituito et al., 2000; *see* Fig. 5*A*, *right panel*). Although Y^{3+} ions were still able to mediate a speeding in the apparent time course of inactivation following coexpression of the rat β_{2a} subunit, this effect was dramatically attenuated compared with that seen in the presence of β_{1b}. Moreover, the speeding did not extend throughout the complete waveform, leaving a large, non-inactivating current component. By contrast, the effects of Y^{3+} on peak current amplitude were enhanced in the presence of β_{2a}, resulting in a threefold decrease in the IC_{50} for peak current block (Fig. 5*C*), further supporting our contention that peak current inhibition and the speeding effect are due to separate mechanisms.

To further corroborate a putative Y^{3+} action on the inactivation machinery, we examined Y^{3+} block of an inactivation-deficient α_{1C} calcium-channel chimera in which the first two thirds of the I-II linker region has been replaced by corresponding α_{1E} sequence. As we have reported recently, this construct (termed CecCCC) exhibits dramatically slowed inactivation kinetics, while its voltage dependence of inactivation is no different than that of the wild type α_{1C} channels (Stotz & Zamponi, 2001). As evident from Fig. 6*A*, CecCCC currents show only little if any Y^{3+}-induced speeding of inactivation kinetics,

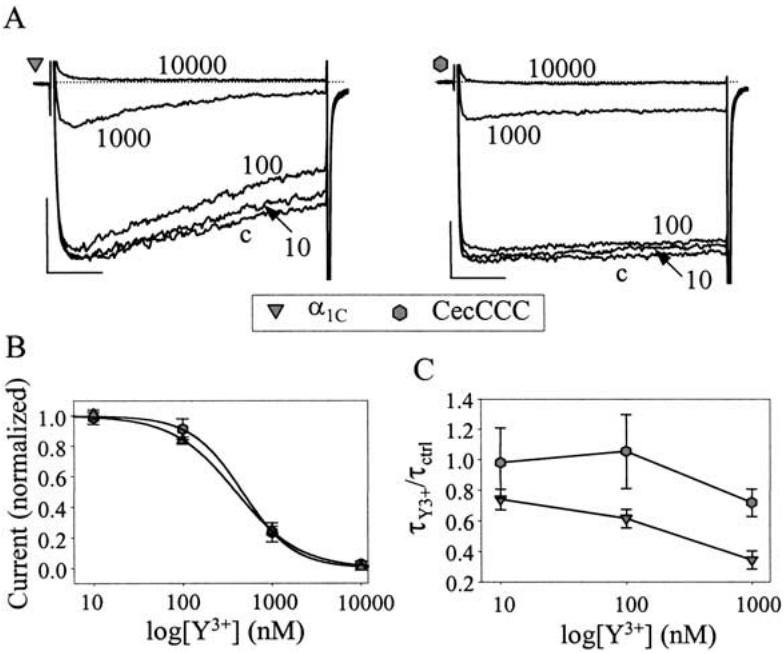

Fig. 6. Effects of Y^{3+} on L-type channels. (*A*) Current records illustrating Y^{3+} block of wild-type α_{1C} L-type channel and a modified L-type channel with ultra slow inactivation kinetics, CecCCC. All records were evoked by step pulses to +10 mV. "c" indicates control current, while numbers denote the concentration of Y^{3+} (nM). Scale bars for both sets of currents are: vertical, 100 pA; horizontal, 30 msec. (*B*) Dose-response curves for α_{1C} and CecCCC. The data were fitted with the Hill equation (α_{1C}: IC_{50} = 391.2 nM, n_h = 1.2, n = 6 to 12; CecCCC: IC_{50} = 462.5 nM, n_h = 1.5, n = 5 to 7). (*C*) Changes in current kinetics in response to Y^{3+} application (n = 3 to 6). Note that the slowly inactivating CecCCC calcium channel undergoes less kinetic speeding than the wild-type α_{1C} channel.

while the sensitivity to peak current block by Y^{3+} is not altered (Fig. 6*B*). Combined kinetic data in Fig. 6*C* reveal that the apparent inactivation rates seen with wild type α_{1C} channels increase as Y^{3+} concentration is increased from 10 nM to 1 μM, whereas for CecCCC currents, a significant speeding is only seen in the presence of 1 μM Y^{3+}. Together with the data obtained in the presence of the β_{2a} subunit, this strongly suggests that Y^{3+} can selectively promote entry into the inactivated states of α_{1A} and α_{1C} calcium channels.

Overall, our data indicate that M^{3+} cations mediate a poorly selective peak current inhibition of all calcium channel subtypes tested, and a more specific acceleration of the macroscopic time course of inactivation of L-type and P/Q-type calcium channels that appears to be governed by a distinct molecular mechanism involving the inactivation gate.

Discussion

This is the first comprehensive study of M^{3+} block on an identified calcium channel species in isolation. All block by M^{3+} species was concentration-dependent and partially reversible. While numerous studies report having to add EGTA to the external solution in order to achieve recovery from M^{3+} block (Triggle & Triggle, 1976; Biagi & Enyeart, 1990; Mlinar & Enyeart, 1993; but *see* Akaike et al., 1989b), this was not necessary in our experiments; however, block reversed only following prolonged washout. In general, we found that our IC_{50}s for M^{3+} species were lower than those previously reported (Akaike et al., 1989a, 1989b; Boland et al., 1991; Reichling & MacDermott, 1991; Mlinar & Enyeart, 1993; Todorovic & Lingle, 1998; but *see* Block et al., 1998). This is most likely related to our use of 2 mM external charge carrier, as most previous studies employed 10 mM or higher concentrations of barium or calcium. Contrary to studies comparing low-voltage-activated and high-voltage-activated currents in neuroblastoma cells and smooth muscle cells, we did not find that high voltage activated currents were more sensitive to M^{3+} block than T-type channels (Narahashi et al., 1987; Akaike et al., 1989a). This could be due to a number of reasons, such as the presence of particular calcium channel splice isoforms or particular calcium channel β subunits expressed in these cells. This underlines the importance of studying M^{3+} block on individual identified calcium channels under identical conditions.

Lanthanides as Structural Probes

The trivalent cations, yttrium (Y^{3+}), lanthanum (La^{3+}), and the lanthanides, are similar in ionic radius, coordination number, and chemistry to calcium and, thus, often have the ability to interact with calcium binding sites (Nieboer, 1975). It is perhaps not surprising that M^{3+} species may interact with the calcium-binding sites along the permeation pathway of calcium channels. Sc^{3+}, Y^{3+}, and La^{3+} are transition metals with electrons in progressively distant outer orbitals and increasing ionic radius as we progress down the periodic table. The lanthanide series, which does not include La^{3+} itself, shares the same outer electron orbital configuration as La^{3+} while adding additional electrons to the "4f" orbitals. Thus, the lanthanides provide an excellent tool to

probe the channel pore as the effective ionic radius decreases across the series (in steps of less than 0.1 Å, a phenomenon known as the lanthanide contraction), while outer electron valence structure remains the same.

In this study, we found a weak inverse correlation between efficacy and ionic radius of the lanthanide series, which was bolstered by the inclusion of Y^{3+} and La^{3+} data. Upon careful examination, we find that it is primarily Ce^{3+} and Yb^{3+} that disrupt this relationship, with Ce^{3+} blocking more and Yb^{3+} blocking less than expected if block is solely dependent on ionic radius. Interestingly, both cerium and ytterbium have multiple oxidation states in aqueous solution, and may be present as Ce^{4+} and Yb^{2+} (Cotton, Wilkinson & Gaus, 1995). While we have no direct evidence for such species in our solutions, it is intriguing to speculate that the Ce^{4+} and Yb^{2+} might increase and decrease blocking affinity, respectively. Alternatively, the departure from the trend of efficacy versus ionic radius by these two species may indicate a lower or higher incidence of hydrolysis products in solution.

Previous studies have also shown an inverse correlation between ionic radius and IC_{50} (Triggle & Triggle, 1976; Mlinar & Enyeart, 1993). However, this correlation does not appear to apply to the smallest M^{3+} species. In thyroid C cells, T-type current inhibition, while inversely correlated with radius for the larger lanthanides, was not significantly different among the small Ho^{3+}, Y^{3+}, Yb^{3+}, and Er^{3+} species (Mlinar & Enyeart, 1993). On the other hand, Triggle and Triggle found that blocking affinity for smooth muscle L-type channels increased from La^{3+} to Tm^{3+} (between Er^{3+} and Yb^{3+}) but decreased with the two smallest lanthanides (Triggle & Triggle, 1976). This finding could also explain why Yb^{3+} block in our experiments was less than expected. In single-channel studies both the entry and exit rates for lanthanides interacting with L-type channels were slowed as lanthanide radius decreased (Lansman, 1990). This suggests that, while it may take more time for the smaller lanthanides to shed their hydration shells, the dependence of affinity on ionic radius may occur because the smaller cations bind more tightly to the channel as indicated by slower exit rates.

Mechanisms of Trivalent Block

Block of calcium channel current by divalent and trivalent cations such as Ni^{2+}, Cd^{2+}, and Ho^{3+} is dependent on both the concentration and the identity of external charge carrier with decreasing block as concentration increases or calcium is substituted for barium (Mlinar & Enyeart, 1993; Zamponi, Bourinet & Snutch, 1996; Lacinova, Klugbauer & Hofmann, 2000). Our experiments with Y^{3+} are consistent with these results. Notably, our finding that peak current block of outward cesium currents by Y^{3+} is weaker than that of inward currents suggests that Y^{3+} ions may be dislodged from their blocking site by permeating cesium ions. Combined, the inhibition of peak current amplitude is consistent with an $M^{2+/3+}$ pore-blocking mechanism. Based on the resolution of discrete lanthanide and divalent blocking events in single-channel studies (Lansman et al., 1986; Lansman, 1990), it seems likely that these ions enter the open channel and physically occlude current flow. However, our finding of a 25-fold decrease in IC_{50} for α_{1G} and a 17-fold decrease in α_{1A} IC_{50} with a 10-fold increase in barium is much greater than that found for Ho^{3+} and Ni^{2+} where approximately 5-fold decreases in affinity were associated with 5-fold increases in calcium or barium concentration (Mlinar & Enyeart, 1993; Serrano et al., 1999). Thus, we expect that part of this shift in Y^{3+} IC_{50} is mediated by an increase in surface charge screening in 20 mM barium. This idea is supported by Block et al., who reported that La^{3+} block of N-type channels is sensitive to charge screening by different concentrations of NMG (a 10-fold increase in extracellular monovalent charge led to a 2.4-fold decrease in La^{3+} IC_{50}; Block et al., 1998). While we did compensate for the change in external charge from 2 to 20 mM barium by altering CsCl concentration, divalent ions screen more effectively than monovalent ions. Thus, we would still expect significant additional screening in 20 mM barium. It is thus likely that the dependence of Y^{3+} potency on external charge carrier reflects two combined processes: increased competition between Y^{3+} and barium within the channel pore, and an increased divalent screening of surface charges near the channel opening that reduces the effective concentration of Y^{3+} near the channel mouth.

Is There a Second M^{3+} Binding Site Outside of the Pore Region?

Several arguments support the notion that peak current inhibition and speeding of channel inactivation kinetics by Y^{3+} are mediated by distinct sites of action. First, in α_{1A} experiments, increasing external charge-carrier concentration antagonized peak current inhibition, but did not affect the Y^{3+}-induced speeding of inactivation kinetics. Second, coexpression of the β_{2a} subunit with α_{1A} enhanced peak current block, but at the same time antagonized the speeding of inactivation kinetics. Third, in the inactivation-deficient L-type channel chimera, peak current block was similar to that seen with wild type channels, whereas the speeding effect was dramatically attenuated. Finally, while peak current block was similar for all channels examined, only the L-type and P/Q-type channels displayed a speeding of current kinetics. Assuming that peak current inhibition is mediated by pore block, this implies that the Y^{3+} target site that is responsible for

the kinetic effects would have to be localized outside of the narrow pore region.

Two lines of experiments support the notion that Y^{3+} ions act by promoting the entry of L-type and P/Q-type channels into the inactivated conformation. First, slowing inactivation via coexpression of the rat β_{2a} subunit limited the ability of Y^{3+} to speed inactivation kinetics. Moreover, in the CecCCC L-type calcium-channel chimera, which displays very slow inactivation under control conditions, Y^{3+} ions were virtually ineffective in changing macroscopic inactivation rates. Thus, our data are consistent with a direct effect of Y^{3+} on L-type and P/Q-type calcium-channel inactivation in addition to the tonic block seen with all types of calcium channels. The molecular mechanism by which this occurs remains enigmatic. We (Stotz & Zamponi, 2001) and others (Kraus et al., 2000; Berjukow et al., 2001) have shown previously that point mutations in the pore-lining S6 segments of the L-type calcium channel α_{1C} subunit (i.e., F823A) can dramatically alter the rates of inactivation. Presumably such changes promote conformational changes in the S6 segments that allow for efficient docking of a cytoplasmic inactivation particle formed by the domain I-II linker. Y^{3+} may mimic the effects of these mutations by promoting similar changes in channel conformation. The absence of any effects of Y^{3+} on the voltage dependence of inactivation parallels our observation with the F823A mutant (Stotz & Zamponi, 2001) that alters the rates of inactivation without affecting steady-state inactivation.

The suggestion of multiple binding sites for multivalent ions is not without precedent. For example, it has been suggested that α_{1E} calcium channels contain a second external nickel binding site that antagonizes channel activation (Zamponi et al., 1996). Moreover, on α_{1A} calcium channels, the presence of an external binding site for calcium linked to the activation gating has been suggested (Zamponi & Snutch, 1996). It is thus conceivable that certain types of voltage-gated calcium channels contain a regulatory site for trivalent metal ions; however, further studies at the molecular level, such as the creation of α_{1A}-α_{1E} chimeras, will be required to confirm the existence of such a site, and to identify its location.

In conclusion, Y^{3+} and the lanthanides are the most potent cationic pore blockers of T-type α_{1G} channels and high-voltage-activated calcium channels described to date. Our work examines, for the first time, the effects of these ions in identified and isolated species of calcium channels, thus allowing the first unequivocal interpretation of the blocking action of these ions. Our novel findings support the notion of a second external Y^{3+} binding site coupled to channel inactivation. While we do not predict the precise location of this site, it may provide interesting insight into our understanding of inactivation mechanisms and how they are conserved among certain channel types (i.e., α_{1C} and α_{1A}).

We thank Dr. Terry Snutch for providing cDNAs encoding the high voltage activated calcium channel subunits. This work was supported by a grant from the Canadian Institutes of Health Research (CIHR) with supplementary funding from the Heart and Stroke Foundation of Alberta and the Northwest Territories. GWZ holds faculty Scholarships from the CIHR, the Alberta Heritage Foundation for Medical Research (AHFMR), and the EJLB Foundation. AMB is the recipient of studentship awards from the AHFMR, the Natural Science and Engineering Research Council, and the Neuroscience Canada Foundation.

References

Akaike, N., Kanaide, H., Kuga, T., Nakamura, M., Sadoshima, J., Tomoike, H. 1989a. Low-voltage-activated calcium current in rat aorta smooth muscle cells in primary culture. *J. Physiol.* **416:**141–160

Akaike, N., Kostyuk, P.G., Osipchuk, Y.V. 1989b. Dihydropyridine-sensitive low-threshold calcium channels in isolated rat hypothalamic neurones. *J. Physiol.* **412:**181–195

Bal, T., McCormick, D.A. 1993. Mechanisms of oscillatory activity in guinea-pig nucleus reticularis thalami in vitro: a mammalian pacemaker. *J. Physiol.* **468:**669–691

Bech-Hansen, N.T., Naylor, M.J., Maybaum, T.A., Pearce, W.G., Koop, B., Fishman, G.A., Mets, M., Musarella, M.A., Boycott, K.M. 1998. Loss-of-function mutations in a calcium-channel alpha1-subunit gene in Xp11.23 cause incomplete X-linked congenital stationary night blindness. *Nat. Genet.* **19:**264–267

Beedle, A.M., Zamponi, G.W. 2000. Block of voltage dependent calcium channels by aliphatic monoamines. *Biophys. J.* **79:**260–270

Beedle, A.M., Zamponi, G.W. 2001. Molecular determinants of opioid analgesia: modulation of presynaptic calcium channels. *Drug Devel. Res.* **54:**118–128

Berjukow, S., Marksteiner, R., Sokolov, S., Weiss, R.G., Margreiter, E., Hering, S. 2001. Amino acids in segment IVS6 and beta-subunit interaction support distinct conformational changes during Ca(v)2.1 inactivation. *J. Biol. Chem.* **276:**17076–17082

Biagi, B.A., Enyeart, J.J. 1990. Gadolinium blocks low- and high-threshold calcium currents in pituitary cells. *Am. J. Physiol.* **259:**C515–C520

Block, B.M., Stacey, W.C., Jones, S.W. 1998. Surface charge and lanthanum block of calcium current in bullfrog sympathetic neurons. *Biophys. J.* **74:**2278–2284

Boland, L.M., Brown, T.A., Dingledine, R. 1991. Gadolinium block of calcium channels: influence of bicarbonate. *Brain Res.* **563:**142–150

Cotton, F.A., Wilkinson, G., Gaus, P.L. 1995. Basic inorganic chemistry. John Wiley & Sons, Toronto

Cribbs, L.L., Gomora, J.C., Daud, A.N., Lee, J.H., Perez-Reyes, E. 2000. Molecular cloning and functional expression of Ca(v)3.1c, a T-type calcium channel from human brain. *FEBS Lett.* **466:**54–58

Cribbs, L.L., Lee, J.H., Yang, J., Satin, J., Zhang, Y., Daud, A., Barclay, J., Williamson, M.P., Fox, M., Rees, M., Perez-Reyes, E. 1998. Cloning and characterization of alpha1H from human heart, a member of the T-type Ca^{2+} channel gene family. *Circ. Res.* **83:**103–109

Deschenes, M., Roy, J.P., Steriade, M. 1982. Thalamic bursting mechanism: an inward slow current revealed by membrane hyperpolarization. *Brain Res.* **239:**289–293

Dubel, S.J., Starr, T.V., Hell, J., Ahlijanian, M.K., Enyeart, J.J., Catterall, W.A., Snutch, T.P. 1992. Molecular cloning of the alpha-1 subunit of an omega-conotoxin-sensitive calcium channel. *Proc. Natl. Acad. Sci. USA.* **89:**5058–5062

Ellis, S.B., Williams, M.E., Ways, N.R., Brenner, R., Sharp, A.H., Leung, A.T., Campbell, K.P., McKenna, E., Koch, W.J., Hui, A. 1988. Sequence and expression of mRNAs encoding the alpha 1 and alpha 2 subunits of a DHP-sensitive calcium channel. *Science* **241:**1661–1664

Hess, P., Lansman, J.B., Tsien, R.W. 1986. Calcium channel selectivity for divalent and monovalent cations. Voltage and concentration dependence of single channel current in ventricular heart cells. *J. Gen. Physiol.* **88:**293–319

Hui, A., Ellinor, P.T., Krizanova, O., Wang, J.J., Diebold, R.J., Schwartz, A. 1991. Molecular cloning of multiple subtypes of a novel rat brain isoform of the alpha 1 subunit of the voltage-dependent calcium channel. Neuron **7:**35–44

Kim, D., Song, I., Keum, S., Lee, T., Jeong, M., Kim, S., McEnery, M.W., Shin, H. 2001. Lack of the burst firing of thalamocortical relay neurons and resistance to absence seizures in mice lacking alpha(1G) T-type Ca(2+) channels. Neuron **31:**35–45

Kraus, R.L., Sinnegger, M.J., Koschak, A., Glossmann, H., Stenirri, S., Carrera, P., Striessnig, J. 2000. Three new familial hemiplegic migraine mutants affect P/Q-type Ca(2+) channel kinetics. *J. Biol. Chem.* **275:**9239–9243

Lacinova, L., Klugbauer, N., Hofmann, F. 2000. Regulation of the calcium channel alpha(1G) subunit by divalent cations and organic blockers. *Neuropharmacology* **39:**1254–1266

Lansman, J.B. 1990. Blockade of current through single calcium channels by trivalent lanthanide cations. Effect of ionic radius on the rates of ion entry and exit. *J. Gen. Physiol.* **95:**679–696

Lansman, J.B., Hess, P., Tsien, R.W. 1986. Blockade of current through single calcium channels by Cd^{2+}, Mg^{2+}, and Ca^{2+}. Voltage and concentration dependence of calcium entry into the pore. *J. Gen. Physiol.* **88:**321–347

Lee, J.H., Daud, A.N., Cribbs, L.L., Lacerda, A.E., Pereverzev, A., Klockner, U., Schneider, T., Perez-Reyes, E. 1999a. Cloning and expression of a novel member of the low voltage-activated T-type calcium channel family. *J. Neurosci.* **19:**1912–1921

Lee, J.H., Gomora, J.C., Cribbs, L.L., Perez-Reyes, E. 1999b. Nickel block of three cloned T-type calcium channels: low concentrations selectively block alpha1H. *Biophys. J.* **77:**3034–3042

Magee, J.C., Johnston, D. 1995. Characterization of single voltage-gated Na^{+} and Ca^{2+} channels in apical dendrites of rat CA1 pyramidal neurons. *J. Physiol.* **487:**67–90

McCleskey, E.W. 1994. Calcium channels: cellular roles and molecular mechanisms. *Curr. Opin. Neurobiol.* **4:**304–312

McRory, J.E., Santi, C.M., Hamming, K.S., Mezeyova, J., Sutton, K.G., Baillie, D.L., Stea, A., Snutch, T.P. 2001. Molecular and functional characterization of a family of rat brain T-type calcium channels. *J. Biol. Chem.* **276:**3999–4011

Mikami, A., Imoto, K., Tanabe, T., Niidome, T., Mori, Y., Takeshima, H., Narumiya, S., Numa, S. 1989. Primary structure and functional expression of the cardiac dihydropyridine-sensitive calcium channel. *Nature* **340:**230–233

Mlinar, B., Enyeart, J.J. 1993. Block of current through T-type calcium channels by trivalent metal cations and nickel in neural rat and human cells. *J. Physiol.* **469:**639–652

Monteil, A., Chemin, J., Bourinet, E., Mennessier, G., Lory, P., Nargeot, J. 2000a. Molecular and functional properties of the human alpha(1G) subunit that forms T-type calcium channels. *J. Biol. Chem.* **275:**6090–6100

Monteil, A., Chemin, J., Leuranguer, V., Altier, C., Mennessier, G., Bourinet, E., Lory, P., Nargeot, J. 2000b. Specific properties of T-type calcium channels generated by the human alpha 1I subunit. *J. Biol. Chem.* **275:**16530–16535

Mori, Y., Friedrich, T., Kim, M.S., Mikami, A., Nakai, J., Ruth, P., Bosse, E., Hofmann, F., Flockerzi, V., Furuichi, T. 1991. Primary structure and functional expression from complementary DNA of a brain calcium channel. *Nature.* **350:**398–402

Narahashi, T., Tsunoo, A., Yoshii, M. 1987. Characterization of two types of calcium channels in mouse neuroblastoma cells. *J. Physiol.* **383:**231–249

Nieboer, E. 1975. The lanthanide ions as structural probes in biological and model systems. *Structure and Bonding.* **22:**1–47

Perez-Reyes, E., Cribbs, L.L., Daud, A., Lacerda, A.E., Barclay, J., Williamson, M.P., Fox, M., Rees, M., Lee, J.H. 1998. Molecular characterization of a neuronal low-voltage-activated T-type calcium channel. *Nature.* **391:**896–900

Reichling, D.B., MacDermott, A.B. 1991. Lanthanum actions on excitatory amino acid-gated currents and voltage-gated calcium currents in rat dorsal horn neurons. *J. Physiol.* **41:**199–218

Restituito, S., Cens, T., Barrere, C., Geib, S., Galas, S., De Waard, M., Charnet, P. 2000. The β2a subunit is a molecular groom for the Ca^{2+} channel inactivation gate. *J. Neurosci.* **20:**9046–9052

Roullet, J.B., Spaetgens, R.L., Burlingame, T., Feng, Z.P., Zamponi, G.W. 1999. Modulation of neuronal voltage-gated calcium channels by farnesol. *J. Biol. Chem.* **274:**25439–25446

Serrano, J.R., Perez-Reyes, E., Jones, S.W. 1999. State-dependent inactivation of the alpha1G T-type calcium channel. *J. Gen. Physiol.* **114:**185–201

Snutch, T.P., Tomlinson, W.J., Leonard, J.P., Gilbert, M.M. 1991. Distinct calcium channels are generated by alternative splicing and are differentially expressed in the mammalian CNS. Neuron. **7:**45–57

Stea, A., Tomlinson, W.J., Soong, T.W., Bourinet, E., Dubel, S.J., Vincent, S.R., Snutch, T.P. 1994. Localization and functional properties of a rat brain alpha 1A calcium channel reflect similarities to Neuronal Q- and P-type channels. *Proc. Natl. Acad. Sci. USA.* **91:**10576–10580

Stotz, S.C., Zamponi, G.W. 2001. Identification of inactivation determinants in the domain IIS6 region of high voltage activated calcium channels. *J. Biol. Chem.* **276:**33001–33010

Todorovic, S.M., Lingle, C.J. 1998. Pharmacological properties of T-type Ca^{2+} current in adult rat sensory neurons: effects of anticonvulsant and anesthetic agents. *J. Neurophysiol.* **79:**240–252

Triggle, C.R., Triggle, D.J. 1976. An analysis of the action of cations of the lanthanide series on the mechanical responses of guinea-pig ileal longitudinal muscle. *J. Physiol.* **254:**39–54

Tsakiridou, E., Bertollini, L., de Curtis, M., Avanzini, G., Pape, H.C. 1995. Selective increase in T-type calcium conductance of reticular thalamic neurons in a rat model of absence epilepsy. *J. Neurosci.* **15:**3110–3117

van Luijtelaar, G., Wiaderna, D., Elants, C., Scheenen, W. 2000. Opposite effects of T- and L-type Ca(2+) channel blockers in generalized absence epilepsy. *Eur. J. Pharmacol.* **406:**381–389

Westenbroek, R.E., Sakurai, T., Elliott, E.M., Hell, J.W., Starr, T.V., Snutch, T.P., Catterall, W.A. 1995. Immunochemical identification and subcellular distribution of the alpha 1A subunits of brain calcium channels. *J. Neurosci.* **15:**6403–6418

Williams, M.E., Brust, P.P., Feldman, D.H., Patthi, S., Simerson, S., Maroufi, A., McCue, A.F., Velicelebi, G., Ellis, S.B., Harpold, M.M. 1992a. Structure and functional expression of an omega-conotoxin-sensitive human N-type calcium channel. *Science.* **257:**389–395

Williams, M.E., Feldman, D.H., McCue, A.F., Brenner, R., Velicelebi, G., Ellis, S.B., Harpold, M.M. 1992b. Structure and functional expression of alpha 1, alpha 2, and beta subunits of a novel human neuronal calcium channel subtype. Neuron. **8:**71–84

Zamponi, G.W., Bourinet, E., Snutch, T.P. 1996. Nickel block of a family of neuronal calcium channels: subtype- and subunit-dependent action at multiple sites. *J. Membrane Biol.* **151:**77–90

Zamponi, G.W., Snutch, T.P. 1996. Evidence for a specific site for modulation of calcium channel activation by external calcium ions. *Pfluegers Arch.* **431:**470–472

Zhang, J.F., Randall, A.D., Ellinor, P.T., Home, W.A., Sather, W.A., Tanabe, T., Schwarz, T.L., Tsien, R.W. 1993. Distinctive pharmacology and kinetics of cloned neuronal Ca^{2+} channels and their possible counterparts in mammalian CNS neurons. *Neuropharmacology*. **32:**1075–1088